ISA Transactions 139 (2023) 391–405

Contents lists available at ScienceDirect

ISA Transactions

journal homepage: www.elsevier.com/locate/isatrans

Research article

SIRSi-vaccine dynamical model for the Covid-19 pandemic☆

Cristiane M. Batistela [a], Diego P.F. Correa [a], Átila M. Bueno [b], José Roberto Castilho Piqueira [b,*]

[a] Federal University of ABC – UFABC – São Bernardo do Campo, SP, Brazil
[b] Polytechnic School of University of São Paulo, São Paulo, SP, Brazil

ARTICLE INFO

Article history:
Received 29 September 2022
Received in revised form 17 April 2023
Accepted 12 May 2023
Available online 16 May 2023

Dataset link: https://github.com/dferruzzo/Covid-19.git

Keywords:
Compartmental model
Equilibrium analysis
Parameter fitting
Social distancing
Vaccination
Bifurcation map

ABSTRACT

Covid-19, caused by severe acute respiratory syndrome coronavirus 2, broke out as a pandemic during the beginning of 2020. The rapid spread of the disease prompted an unprecedented global response involving academic institutions, regulatory agencies, and industries. Vaccination and nonpharmaceutical interventions including social distancing have proven to be the most effective strategies to combat the pandemic. In this context, it is crucial to understand the dynamic behavior of the Covid-19 spread together with possible vaccination strategies. In this study, a susceptible–infected–removed–sick model with vaccination (SIRSi-vaccine) was proposed, accounting for the unreported yet infectious. The model considered the possibility of temporary immunity following infection or vaccination. Both situations contribute toward the spread of diseases. The transcritical bifurcation diagram of alternating and mutually exclusive stabilities for both disease-free and endemic equilibria were determined in the parameter space of vaccination rate and isolation index. The existing equilibrium conditions for both points were determined in terms of the epidemiological parameters of the model. The bifurcation diagram allowed us to estimate the maximum number of confirmed cases expected for each set of parameters. The model was fitted with data from São Paulo, the state capital of SP, Brazil, which describes the number of confirmed infected cases and the isolation index for the considered data window. Furthermore, simulation results demonstrate the possibility of periodic undamped oscillatory behavior of the susceptible population and the number of confirmed cases forced by the periodic small-amplitude oscillations in the isolation index. The main contributions of the proposed model are as follows: A minimum effort was required when vaccination was combined with social isolation, while additionally ensuring the existence of equilibrium points. The model could provide valuable information for policymakers, helping define disease prevention mitigation strategies that combine vaccination and non-pharmaceutical interventions, such as social distancing and the use of masks. In addition, the SIRSi-vaccine model facilitated the qualitative assessment of information regarding the unreported infected yet infectious cases, while considering temporary immunity, vaccination, and social isolation index.

1. Introduction

On January 30, 2020, the World Health Organization (WHO) declared a public health emergency of international concern (PHEIC). Four weeks prior to that, the Wuhan Municipal Health Commission had reported a cluster of pneumonia Cases, for which the causative agent was identified as the severe acute respiratory syndrome coronavirus 2 (SARS-CoV-2), and the disease was named Covid-19. Following the WHO alert, Covid-19 was declared a pandemic in March 2020 [1,2]. The rapidly spreading disease challenged healthcare agencies, academic institutions, and industries to develop and deploy efficient vaccines and drug treatments.

Several drugs were tested on patients with Covid-19 unfortunately, the studies [3–7] found marginal or no effect on overall mortality, initiation of ventilation, the duration of hospital stay, or viral clearance, even with chronic use.

On the other hand, non-pharmaceutical interventions (NPIs), including physical distancing, use of facemasks, and eye protection, reduced viral transmissions [8,9]. Populations across the globe were compliant with NPIs; however, in certain countries, their effectiveness fluctuated [10] resulting in hesitancy toward vaccination [11]. In Brazil, the closure of nonessential activities

☆ JRCP is supported by the Brazilian Research Council (CNPq), grant number: 302883/2018-5. AMB is supported by Programa de Apoio aos Novos Docentes USP, grant number: 2022.1.9345.1.2.

* Corresponding author.
E-mail addresses: cristiane.batistela@ufabc.edu.br (C.M. Batistela), diego.ferruzzo@ufabc.edu.br (D.P.F. Correa), atila.bueno@usp.br (Á.M. Bueno), piqueira@lac.usp.br (J.R.C. Piqueira).

https://doi.org/10.1016/j.isatra.2023.05.008
0019-0578/

lasted only for a short time, and NPIs were lifted in cities in an uncoordinated manner [9]. Consequently, the downward trend in the number of Covid-19 cases reversed in November 2020, initiating a second wave of infections [12].

Although vaccine development is considerably expensive and requires several years or decades, Covid-19 vaccines were developed rapidly, owing to the years of prior development of vaccines against similar viruses such as severe acute respiratory syndrome (SARS) and the Middle East respiratory syndrome (MERS). In addition, the experience obtained from combating the Ebola vaccine showed that vaccine development can be accelerated through coordinated global efforts, including those of academic institutions, industries, and healthcare regulatory agencies, without compromising safety [13–15].

To date, more than hundred Covid-19 vaccines have been developed for human clinical trials. Emergency use authorization for Covid-19 vaccines was granted at the beginning of December 2020 by Britain's National Health Service and later by the US Food and Drug Administration (FDA). In January 2021, the Brazilian National Health Surveillance Agency (Anvisa) granted emergency use authorization for Covid-19 vaccines. Currently, 12 vaccines have been approved for human administration in many countries [16,17].

The Covid-19 pandemic and subsequent efforts for vaccination started a race among countries to rapidly vaccinate their populations. Immunization results of nationwide mass vaccination in Israel [18] strengthened the expected mitigation of the Covid-19 pandemic. However, in many countries, a successful vaccination strategy required a lengthy journey [19].

Logistics play an important role in vaccination strategies, requiring nationally coordinated administration, considering the diversity of interventions and local changes in vaccine supply [20]. In addition, the efficacy[1] of the vaccines currently in development and use range between 50.38%–95.0% [16], necessitating different vaccination strategies based on factors such as the number of doses, immunization schedule and specific storage facility requirements.

Healthcare agencies ought to consider new Covid-19 variants and vaccination strategies such as varying the NPI implementation or delaying the second dose to accelerate the first-dose vaccination among the population [21,22]. Vaccine efficacy and population coverage are important factors; vaccines ought to exhibit an efficacy of at least 70% with a population coverage of at least 75% to prevent outbreaks without intervention. The pandemic is expected to dwindle after attaining a vaccine efficacy of at least 80% with vaccination administered to a population of 75% [23].

Provided this complex context, to attenuate the ongoing pandemic, it is important to understand the dynamic behavior of the Covid-19 pandemic, considering possible vaccination strategies.

Epidemiological models are important tools in the decision-making process for establishing regional or national health policies, helping answer questions such as: when will the next peak of infections occur? Is social distancing an effective strategy? Will the number of new cases and hospitalizations increase or decrease for a given strategy? Moreover, the primary use for epidemiological models is to estimate the relative effectiveness of various interventions [24].

No model can perfectly predict the spread of a disease. However, approximations with low uncertainties can be useful in designing public health policies. For instance, short-term forecasting is important for planning hospital bed numbers; long-term forecasts in this case are usually unnecessary. Every epidemiological model is built on assumptions that allow for simplifications. As a general rule, oversimplified models cannot capture complex behaviors in the dynamics of a diseases. However, complex models can be deceitful and generate an impression of realism while concealing crucial information [24,25].

Usually, epidemiological models involve such as considering a homogeneous population, which means that every individual exhibits an equal probability of contact with each other, and assumes a constant population with no births or migration. In many cases, the models do not consider the latent period after an individual is exposed or infected by the disease, but is not yet infectious [24].

Since the onset of the pandemic, many scientific studies have focused toward mitigating the pandemic. These studies include control system strategies deep learning modeling, mathematical modeling analysis, social networks, game theory, and numerical simulations, to predict the contagious behavior of Covid-19and to arrive at vaccination strategies.

Arunkumar et al. [26] proposed two time-series models for the COVID-19 pandemic: the autoregressive integrated moving average (ARIMA) and seasonal auto-regressive integrated moving average (SARIMA) models were developed using data from different countries accounting for 70%–80% of the global cumulative cases. The results for the worst-case scenarios showed a possible exponential growth in the number of confirmed cases and deaths. However, the primary limitation of this study was related to the strong uncertainties in the model parameters, resulting in a wide range of possible future trajectories, and impaired long-term forecasting.

Fiacchini et al. [27] proposed a simple two-parameter two-dimensional model developed to reproduce the time-series of daily deaths and hospitalizations in France. Despite its simplicity, the model reproduced the general behavioral trends of the time-series.

An interesting epidemiological model was presented by Markovič et al. [28]. A computational model was developed for a social network, allowing the study of Covid-19 epidemics in heterogeneous populations. Social networks were considered to comprise subpopulations with different economic statuses, health conditions (comorbidities), and ages. An extended SEIRS model was used to explore the influence of these aspects on the progression of Covid-19. They highlighted that the spatial configuration could be a determinant of the development of the disease; they concluded that in a healthier society, the disease may spread rapidly, however with less severe consequences. The advantages of considering complex patterns of interactions and the heterogeneity of the population showed that different from the public vaccination policies widely adopted, if vaccination is limited and demographic distribution in the social network is homogeneous, better epidemic results can be achieved, assuming that the healthy individuals are vaccinated first, rather than prioritizing the elderly and other risk groups.

Game theory and social network models can be used for such decision-making regarding the best policies for vaccination programs. Piraveenan et al. [29] coupled game theory with social network analysis and agent-based techniques to model the population and simulate the dynamics of Covid-19. Game theory modeling considered two components: the decision-making process of individuals receiving the vaccine, and the administrative process associated with governments and policymakers in selecting the population groups to be vaccinated, provided the initial dose limitations. The former component is an influenced by factors such as demography, physical location, and health. The latter component is influenced by factors such as the epidemic parameters, logistics, and human resources. The approach provided a roadmap for the implementation of vaccination programs.

[1] Vaccine efficacy is the percentage disease reduction in a vaccinated group in a clinical trial.

The results showed that efficient testing using contact tracing and isolation procedures are important factors for the containment of Covid-19; however, effective vaccination programs and vaccination uptake surpass these factors to mitigate the Covid-19 pandemic regionally and globally.

Tichoumi et al. [30] investigated the co-dynamics of malaria and Covid-19 and a control strategy based on nontherapeutic interventions was proposed to mitigate the propagation of both diseases in the population. The numerical results showed that each disease can be controlled individually; however, better results were obtained when both controls were applied to reduce the number of infections and coinfections.

A susceptible–infected–removed model was used to predict the Covid-19 pandemic in Kuwait [31], the study recommended the extension of preventive measures to control the Covid-19 growth. An SIR-type model with a nonconstant population was developed by Muñoz-Fernández et al. [32]. The model was calibrated using the rates of infection and death in Italy, Spain, and the USA. Several plausible scenarios were investigated, drawing attention to the high transmission rates in the USA. The model was used to investigate the sensitivity to sociological behavioral changes, such as higher mobility and relaxation of individual protection toward measures such as the use of face-masks.

A susceptibility–infected–removed–sick (SIRSi) model was proposed by Batistela et al. [33], considering unreported or asymptomatic cases and the effects of temporary acquired immunity in the Covid-19 propagation. The results revealed the existence of a mutually exclusive disease-free and endemic equilibrium points. As the model accounts for asymptomatic cases, the effects on the pandemic dynamics could be inferred.

In contrast, Zhai et al. [34] showed that reinfection can occur immediately after an infection period, that is, without temporary acquired immunity. The SIR extended model accounts for age heterogeneity in the population using two compartments: S_1 for children of age $<$ 14 years and for the elderly of age $>$ 65 years; S_2 for the population of 14 years $<$ age $<$ 65 years. The results revealed various scenarios, including disease-free endemic and epidemic situations.

Nakamura et al. [35] modeled the death toll owing to the Covid-19 pandemic using a sigmoid curve to predict mortality and estimate values such as the basic reproduction number, that is, the number of new cases per infection. The fitting of the sigmoid curve allowed for the determination of epidemiological parameters from systems of algebraic equations. In addition, the obtained parameters can be used as initial estimates for other optimization algorithms.

Wei et al. [36] developed a susceptible–exposed–quarantined–infected–recovered (SEQIR) mathematical model of Covid-19 and implemented a control system based on the state observers. This control system aimed to reduce the number of susceptible individuals in a population using the NPI strategy. The state-observer approach was an interesting choice for effectively addressing the transmission uncertainties of Covid-19.

A susceptible–infected–recovered–deceased (SIRD) model was developed by Morato et al. [37] and a quarantine strategy was considered for the control of Covid-19 in Brazil. The quarantine strategy was guided by a model-predictive control procedure. As social distancing measures are implemented, the epidemiological parameters vary, which were estimated using an autoregressive integrated moving average (ARIMA) model for forecasting the Covid-19 pandemic in Brazil. The results demonstrated that herd immunity could not be achieved, and that as a coordinated control strategy was not pursued, social distancing measures would continue for a long time.

Ma et al. [38] proposed a generalized SEIR model with fractional-order derivatives. A sensitivity analysis of basic reproduction number R_0 with respect to the epidemiological parameters was performed to rank the critical parameters controlling epidemics. The parameters related to the protection rate, which can be viewed as an ensemble of protective measures, such as social distancing and vaccines, are the most effective Covid-19 control parameters.

Kumar and Kumar [39] developed a fuzzy time series model to forecast the number of deaths owing to Covid-19 pandemic in India. This model facilitates the estimation of the number of hospital beds and the number of intensive care units necessary to manage pandemics in the future.

Several studies have considered deep learning for predicting the number of Covid-19 cases. These studies included a prediction model for the confirmed cases and deaths owing to Covid-19 based on a deep learning algorithm with two long short-term memory layers, considering the data available for Covid-19 in India [40]. Furthermore, multi-layer deep learning models with perceptron, random forest, and long short-term memory, were trained and used for forecasting the Covid-19 pandemic in Iran [41]. In both cases, the models exhibited limitations in terms of data quality as the testing rate varied significantly over time.

Additionally, several studies have considered the dynamics of vaccination strategies. Angeli et al. [42] modeled the effects of a vaccine campaign with the aim of Forecasting the epidemic evolution. The extended SIR model with several parameters and a machine learning method were used to determine the initial conditions. Data from 27 countries were used to study the evolution of the pandemic. The study concluded that herd immunity was probably beyond attainment, highlighting the importance of reducing the infection rate through restrictive measures and vaccination.

Li and Guo [43] considered an imperfect vaccination model to develop control strategies for mutated Covid-19 strains. The control strategy comprised the following steps: imperfect vaccination, isolation, and testing. This study addressed the problem of dynamically adjusting the three control strategies to minimize the number of infections at the lowest cost. A two-strain model was studied by León et al. [44]. They argued that the delta variant was common across many countries, probably because of the high transmission rate in vaccinated individuals and the delay in administration of booster vaccine doses.

A bi-virus competing model was presented by Luo et al. [45], and its stability was studied. When the disease-free equilibrium was unstable, that is, in an ongoing epidemic, two viruses compete, and eventually, one is extinguished and the other becomes dominant.

Yasuda et al. [46] proposed an age-specific epidemic model and studied the impact of vaccination strategies on young (socially active) populations and in older populations with higher health risks. The significance of the study is the consideration of the heterogeneity in the population, considering the differences in social activities related to population age.

The development of predictive tools that consider the science of complexity as a delineator has facilitated significant advances in the dynamics of global epidemics by considering multiple factors believed to be relevant to the context, such as demographic variations, mobility patterns, detailed epidemiological data, and disease characteristics. An important initiative in this direction is the global epidemic and mobility (GLEAM), which provides a simulation framework involving these considerations [47].

Zhai et al. [48] studied the SEIR model and designed the vaccination strategy using a delayed-state feedback linearization technique. The results show the possible control of Covid-19 epidemics in finite time.

Zhai et al. [49] proposed a multi-group SEIIR model, considering two infectious compartments: infectious but not in treatment; infectious and in treatment. The stability of the

disease-free equilibrium was studied. When the disease-free equilibrium was unstable, two control strategies were proposed: increasing the treatment capacity; and increasing the number of tests to remove virus-free population.

In compartmental models, the dissemination of a virus within a population can be described using a system of time-dependent differential equations (dynamic system). In the the current study, the spread of Covid-19 was accordingly, described by a set of differential equations written in a state-space format [50,51].

We modified a previous model [33], and proposed a vaccination strategy for susceptible individuals. The proposed SIRSi-Vaccine model comprises four compartments: susceptible, infected, sick, and recovered. The focus was on assessing the effects of the proposed vaccination together with social distancing as an NPI in the Covid-19 spread dynamics.

The proposed SIRSi-Vaccine model presents both the disease-free and endemic equilibrium points. The equilibrium-point stabilities were studied both analytically and numerically. Consequently, the equilibrium condition was related to the effects of social distancing with the proposed vaccination.

The SIRSi-Vaccine model was numerically adjusted for the epidemic situation in São Paulo, facilitating the development of relationship between the contours of the maximum number of confirmed cases and combination for social distancing index and vaccination rate parameters. In addition, the simulation results indicated the existence of undamped oscillatory behavior in the number of confirmed cases in the susceptible population, driven by a combination of short and long small amplitude periodic oscillations in the social distancing indices.

The proposed model was validated by describing the dynamics of the spread of the disease in the São Paulo state capital city, Brazil. When considering the description of society considering the realities of a global pandemic, or even national or regional scales, complexity science can provide more insightful solutions than conventional approaches [52].

To stop the spread of Covid-19 different strategies, with respect to social distancing and vaccination efforts, may be necessary for different cities.

The remainder of this paper is organized as follows: Sections 2 and 3 present the mathematical models and stability analysis of the equilibrium points. The parametric fitting of the mathematical models are presented in Section 4. The numerical simulation results are presented in Section 5. The limitations of the model are discussed in Section 6. The conclusions are presented in Section 7.

2. SIRSi model

A constant population model with four compartments was proposed (Fig. 1): susceptible (S), infected (I), infected symptomatic positive tested (S_{ick}), and recovered (R). The S_{ick} compartment comprises a group of infected people. Based on the data collected from this group, we concluded that it is possible to adjust the model parameters and assess information regarding the nonreported infected (I), consisting of those infected and infectious, with or without symptoms, however are not notified by public agencies.

The available public data do not consider the spatial connectivity between the individuals in the population, specific information on different viral strains, specific characteristics of mutations, agents with high viral loads, or other intrinsic factors. Therefore, considering homogeneous population appears to be an effective way to develop the model. SIR models are based on a macroscopic view of the transmission of an infectious disease in a specific population, allowing for a qualitative study of the disease [24,25]. Provided these aspects, the proposed SIRSi model considers a homogeneous population, that is, all individuals have the same probability to acquire or transmit the disease independently of age, health, or economic condition. Additionally, the model assumes a closed population, without migration. Furthermore, characteristics such as the latency period, which depend on the availability of data, or viral mutations could not be considered.

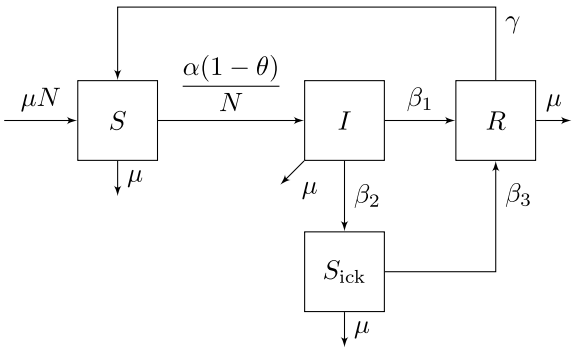

Fig. 1. Block diagram for the compartmental SIRSi model in Eqs. (2.2). The model consists of four compartments: susceptible (S), infected (I), infected symptomatic positive tested (S_{ick}) and recovered (R). The arrows indicate the flow of individuals between compartments, with infection rate ($\alpha(1-\theta)/N$) and recovery rate (β_1) governing the transition between infected asymptomatic and recovered compartments. The model assumes equal rates of births and deaths, and individuals who recover from the infection become completely susceptible to the disease again at a certain rate, represented as (γ).

In Fig. 1, I is the infectious population compartment representing the population in the incubation stage (prior to symptom onset). Zou et al. [53–55] reported the transmission during this period.

Many infectious diseases present an exposed or latent period before the development of symptoms. This is reflected in the susceptible–exposed–infected–recovered (SEIR) models [56,57], where the exposed compartment comprises infected individuals that are not yet infectious, that is, not yet transmitting the disease. To avoid the escalation of complexity in the model, we assumed that the infected individuals are already infectious.

Covid-19 is peculiar, because a fraction of the infected population will never present any symptom throughout the course of the disease. In addition, there are still unanswered questions on the transmission rate of the asymptomatic compared to the symptomatic individuals, and consequently, the role of asymptomatic individuals is a key question in the evolution of the pandemic. Therefore, the model presented in Fig. 1 considers the influence of asymptomatic individuals in the spread of Covid-19 [33].

Despite the peculiarity of Covid-19, considering that asymptomatic infected people, represented by the compartment I, contribute to the dynamics of virus propagation, the model that is validated with data from the reported infected people, (S_{ick}), facilitates the assessment of information regarding the non symptomatic people (I), which is a relevant characteristic of the proposed study. Additionally, the proposed model allows the study of the efficiency of strategies combining vaccination and the isolation index for formulating health policy aiming to mitigate the Covid-19 spread.

Those who are asymptomatic or do not develop severe symptoms, that is, cases that are neither tested nor documented, are moved to the $R(t)$ (recovered) compartment at a rate of β_1 [33].

β_2 is the rate at which infected individuals develop symptoms or are tested positive. Therefore, the $S_{\text{ick}}(t)$ compartment comprises individuals with more severe symptoms, seeking medical attention and adopting more stringent NPI such as quarantine.

Individuals in the $S_{\text{ick}}(t)$ compartment who recover are shifted to the $R(t)$ compartment at a rate β_3.

The possibility of temporary immunity for recovered individuals [33,58–60], was additionally considered. As shown in Fig. 1, the recovered (R) population becomes susceptible (S) again at a rate of γ.

The model was developed considering the population size constraint in Eq. (2.1). The population growth and death rates μ, including deaths because of Covid-19 were similar in the state of São Paulo [61]; therefore, in this study, they were considered to be equal.

$$N = S(t) + I(t) + S_{\text{ick}}(t) + R(t). \tag{2.1}$$

From these considerations, the SIRSi mathematical model is given by Eq. (2.2).

$$\begin{aligned}
\frac{d}{dt}S(t) &= \mu N - \frac{\alpha(1-\theta)}{N}S(t)I(t) - \mu S(t) + \gamma R(t);\\
\frac{d}{dt}I(t) &= \frac{\alpha(1-\theta)}{N}S(t)I(t) - (\beta_1+\beta_2)I(t) - \mu I(t);\\
\frac{d}{dt}S_{\text{ick}}(t) &= \beta_2 I(t) - \beta_3 S_{\text{ick}}(t) - \mu S_{\text{ick}}(t);\\
\frac{d}{dt}R(t) &= \beta_1 I(t) + \beta_3 S_{\text{ick}}(t) - \gamma R(t) - \mu R(t).
\end{aligned} \tag{2.2}$$

In Eq. (2.2), the effect of social distancing measures, a form of NPI, was introduced by the parameter $\theta \in [0, 1]$; $\theta = 0$ indicates that no social distancing measure was under consideration, whereas $\theta = 1$ indicates a complete lock-down.

Normalization with respect to the population size N was performed using Eq. (2.1), resulting in Eq. (2.3),

$$1 = s(t) + i(t) + s_{\text{ick}}(t) + r(t), \tag{2.3}$$

where $s(t) = S(t)/N$, $i(t) = I(t)/N$, $s_{\text{ick}}(t) = S_{\text{ick}}(t)/N$, and $r(t) = R(t)/N$. Replacing Eq. (2.3) into the system of Eq. (2.2), yields Eq. (2.4).

$$\begin{aligned}
\frac{d}{dt}s(t) &= \mu - \alpha(1-\theta)si - \mu s + \gamma r;\\
\frac{d}{dt}i(t) &= \alpha(1-\theta)si - (\beta_1+\beta_2)i - \mu i;\\
\frac{d}{dt}s_{\text{ick}}(t) &= \beta_2 i - \beta_3 s_{\text{ick}} - \mu s_{\text{ick}};\\
\frac{d}{dt}r(t) &= \beta_1 i + \beta_3 s_{\text{ick}} - \gamma r - \mu r.
\end{aligned} \tag{2.4}$$

In addition, from Eq. (2.3), the recovered compartment $r(t)$ can be written as a linear combination of other compartments (or state variables), as shown in Eq. (2.5):

$$r(t) = 1 - s(t) - i(t) - s_{\text{ick}}(t). \tag{2.5}$$

Consequently, the solutions

$$\Omega = \{(s(t), i(t), s_{\text{ick}}(t)) \in \mathbb{R}^3_+ \mid s(t) + i(t) + s_{\text{ick}}(t) \leq 1\}$$

of Eq. (2.4) can be studied in the system of Eq. (2.6):

$$\begin{aligned}
\frac{d}{dt}s(t) &= \mu + \gamma - \alpha(1-\theta)si - (\mu+\gamma)s - \gamma i - \gamma s_{\text{ick}};\\
\frac{d}{dt}i(t) &= \alpha(1-\theta)si - (\beta_1+\beta_2+\mu)i;\\
\frac{d}{dt}s_{\text{ick}}(t) &= \beta_2 i - (\beta_3+\mu)s_{\text{ick}}.
\end{aligned} \tag{2.6}$$

This model was studied by Batistela et al. [33]. The basic reproduction number is given by:

$$R_0 = \frac{\alpha(1-\theta)}{\beta_1+\beta_2+\mu}, \tag{2.7}$$

which represents whether or not the disease will thrive; and rate of spread, if at least one infected individual appears in the population.

2.1. SIRSi equilibrium points

The system of Eq. (2.6) contains two equilibrium points: one is consistent with a disease-free situation, and the other represents an endemic equilibrium.

The disease-free equilibrium point P_{df1} is given by Eq. (2.8).

$$P_{df1} = \begin{bmatrix} s^* \\ i^* \\ s^*_{\text{ick}} \end{bmatrix} = \begin{bmatrix} 1 \\ 0 \\ 0 \end{bmatrix} \tag{2.8}$$

To analyze the local stability of the equilibrium point, the Jacobian matrix J of the system in Eq. (2.6) is shown in Eq. (2.9).

$$J = \begin{bmatrix} -\alpha(1-\theta)i^* - (\mu+\gamma) & -\alpha(1-\theta)s^* - \gamma & -\gamma \\ \alpha(1-\theta)i^* & \alpha(1-\theta)s^* - (\beta_1+\beta_2+\mu) & 0 \\ 0 & \beta_2 & -(\beta_3+\mu) \end{bmatrix} \tag{2.9}$$

The eigenvalues associated with P_{df1} are given by Eq. (2.10).

$$\begin{aligned}
\lambda_1 &= -(\mu+\gamma),\\
\lambda_2 &= (R_0 - 1)(\beta_1+\beta_2+\mu),\\
\lambda_3 &= -(\beta_3+\mu).
\end{aligned} \tag{2.10}$$

The eigenvalue λ_2 shows the possibility of a transcritical bifurcation, as it can change sign depending on the value of R_0.

Theorem 1. *The disease-free EP $(s^*, i^*, s^*_{ick}) = (1, 0, 0)$ corresponding to the model without vaccine in (2.6) is locally asymptotically stable, if $R_0 < 1$; and unstable, if $R_0 > 1$.*

Proof. The proof is evident from the definition of the eigenvalue λ_2 in Eq. (2.10). □

The endemic equilibrium point P_{e1} is given by Eq. (2.11):

$$P_{e1} = \begin{bmatrix} s^* \\ i^* \\ s^*_{\text{ick}} \end{bmatrix} = \begin{bmatrix} \frac{1}{R_0} \\ (\beta_3+\mu)\varphi \\ \beta_2\varphi \end{bmatrix}, \tag{2.11}$$

where

$$\varphi = \left(\frac{R_0 - 1}{R_0}\right)\left(\frac{\gamma+\mu}{(\beta_1+\beta_2+\mu)(\beta_3+\mu) + (\beta_2+\beta_3+\mu)\gamma}\right). \tag{2.12}$$

The characteristic polynomial of P_{e1} is given by Eq. (2.13):

$$\mathcal{P}_{e1}(\lambda) = \lambda^3 + a_1\lambda^2 + a_2\lambda + a_3, \tag{2.13}$$

where

$$\begin{aligned}
a_1 &= \varphi\alpha(1-\theta)(\beta_3+\mu) + \beta_3 + \gamma + 2\mu\\
a_2 &= (\beta_3+\mu)[\gamma + \mu + \varphi\alpha(1-\theta)(\beta_1+\beta_2+\beta_3+\gamma+2\mu)]\\
a_3 &= \varphi\alpha(1-\theta)(\beta_3+\mu)(\beta_1\beta_3 + \beta_1\mu + \beta_2\beta_3 + \beta_2\gamma\\
&\quad + \beta_2\mu + \beta_3\gamma + \beta_3\mu + \gamma\mu + \mu^2).
\end{aligned} \tag{2.14}$$

Theorem 2. *The endemic EP $(s^*, i^*, s^*_{ick}) = (1/R_0, (\beta_3+\mu)\varphi, \beta_2\varphi)$ of the system (2.6) is locally asymptotically stable, if $R_0 > 1$; and unstable, if $R_0 < 1$.*

Proof. The coefficients a_1, a_2, and a_3 in Eq. (2.14), are positive real numbers, if $\varphi > 0$ (see Eq. (2.12)). In this case, we determined whether the characteristic polynomial in Eq. (2.13) contains unstable or stable roots, using the Routh–Hurwitz stability criterion [62].

Consequently, the characteristic polynomial in Eq. (2.13) is stable if Eq. (2.15) is satisfied:

$$b_1 = a_2 - \frac{a_3}{a_1} > 0. \tag{2.15}$$

The proof that Eq. (2.15) holds true demands mathematical reasoning, which results in Eq. (2.16):

$$b_1 = \frac{1}{a_1}(\beta_3 + \mu)\left[\varphi^2 c_1^2 c_2 + \varphi c_1 c_3 + c_4\right], \tag{2.16}$$

where

$c_1 = \alpha(1-\theta)$;

$c_2 = (\beta_1+\beta_2)(\beta_3+\mu) + \beta_3^2 + \beta_3\gamma + 3\beta_3\mu + \gamma\mu + 2\mu^2$;

$c_3 = \beta_1\gamma + \beta_1\mu + \beta_2\mu + \beta_3^2 + 2\beta_3\gamma + 4\beta_3\mu + \gamma^2 + 4\gamma\mu + 4\mu^2$;

$c_4 = \beta_3\gamma + \beta_3\mu + \gamma^2 + 3\gamma\mu + 2\mu^2$.

The expression inside the brackets in Eq. (2.16) is positive, if $\varphi > 0$. Consequently, for $\varphi > 0$, Eq. (2.15) holds true, and P_{e1} is asymptotically stable. In addition, as shown in Eq. (2.12), $\varphi > 0$ implies that $R_0 > 1$. □

3. The model with vaccination

In Brazil, vaccines with different efficacy rates have been granted use authorization since 2020. The vaccination rate varies over time in each city, depending on many factors, including the local availability of vaccines, local vaccination rate capability, and the size of the population being vaccinated considering age and health conditions.

The available data do not provide information regarding the types of vaccines administered to the individuals in the population. Considering this, the efficacy of the vaccine cannot be considered for the model validation, and it is considered that all vaccinated individuals are homogeneously immunized, resulting in another limitation of the proposed model.

In most studies, vaccination rate in SIR models were implemented as a constant [63,64]. Therefore, vaccination intervention was introduced in susceptible individuals. Once the individuals are vaccinated, they are moved to the $r(t)$ (recovered) compartment at a rate given by the vaccination effort ω. It is assumed that the vaccination effort will decrease the number of the susceptible individuals in the population. Consequently, it is expected that over time, the number of infected individuals will decrease.

The proposed SIRSi-Vaccine model is illustrated in Fig. 2. Including vaccination intervention in Eqs. (2.4) and (2.6) yields Eqs. (3.1) and (3.2), respectively.

$$\begin{aligned}
\frac{d}{dt}s(t) &= \mu - \alpha(1-\theta)si - \mu s + \gamma r - \omega s;\\
\frac{d}{dt}i(t) &= \alpha(1-\theta)si - (\beta_1+\beta_2)i - \mu i;\\
\frac{d}{dt}s_{\text{ick}}(t) &= \beta_2 i - \beta_3 s_{\text{ick}} - \mu s_{\text{ick}};\\
\frac{dr}{dt}r(t) &= \beta_1 i + \beta_3 s_{\text{ick}} - \gamma r + \omega s - \mu r.
\end{aligned} \tag{3.1}$$

$$\begin{aligned}
\frac{d}{dt}s(t) &= \mu + \gamma - \alpha(1-\theta)si - (\mu+\gamma+\omega)s - \gamma i - \gamma s_{\text{ick}};\\
\frac{d}{dt}i(t) &= \alpha(1-\theta)si - (\beta_1+\beta_2+\mu)i;\\
\frac{d}{dt}s_{\text{ick}}(t) &= \beta_2 i - (\beta_3+\mu)s_{\text{ick}}.
\end{aligned} \tag{3.2}$$

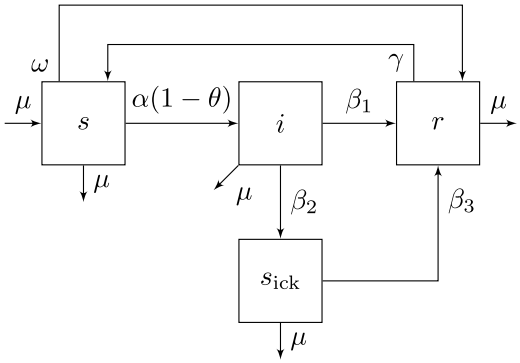

Fig. 2. Schematic of the compartmental SIRSi model with Vaccination, as described by Eq. (3.1), illustrating the flow of individuals through the susceptible (s), infected (i), infected symptomatic (s_{ick}), and recovered (r) compartments in a normalized population. The model considers the effect of vaccination on the transmission dynamics of the disease. The arrows indicate the flow of individuals between compartments, with the rates of transitions determined by the model parameters.

3.1. Basic reproduction number R_0

We obtain R_0 of the disease-free EP using next-generation matrix (NGM) method [65,66]. Therefore, the transmission matrices T and Σ are:

$$T = \begin{bmatrix} 0 & -\dfrac{\alpha(1-\theta)(\mu+\gamma)}{\mu+\gamma+\omega} & 0 \\ 0 & \dfrac{\alpha(1-\theta)(\mu+\gamma)}{\mu+\gamma+\omega} & 0 \\ 0 & 0 & 0 \end{bmatrix},$$
$$\Sigma = \begin{bmatrix} -(\mu+\gamma+\omega) & -\gamma & -\gamma \\ 0 & -(\beta_1+\beta_2+\mu) & 0 \\ 0 & \beta_2 & -(\beta_3+\mu) \end{bmatrix}, \tag{3.3}$$

where R_0 is the largest eigenvalue of the NGM with large domain $K = -T\Sigma^{-1}$:

$$K = \begin{bmatrix} 0 & \dfrac{\alpha(1-\theta)(\gamma+\mu)}{(-\beta_1-\beta_2-\mu)(\gamma+\mu+\omega)} & 0 \\ 0 & -\dfrac{\alpha(1-\theta)(\gamma+\mu)}{(-\beta_1-\beta_2-\mu)(\gamma+\mu+\omega)} & 0 \\ 0 & 0 & 0 \end{bmatrix}. \tag{3.4}$$

Therefore,

$$R_0 = \frac{\alpha(1-\theta)(\mu+\gamma)}{(\beta_1+\beta_2+\mu)(\gamma+\mu+\omega)}. \tag{3.5}$$

3.2. SIRSi-Vaccine equilibrium points

As discussed in Section 2.1, the SIRSi-Vaccine mathematical model in Eq. (3.2) contains two equilibrium points: the first of which is consistent with a disease-free scenario; and the other with an endemic equilibrium.

The disease-free equilibrium point in Eq. (3.2) is shown in Eq. (3.6), for $s^* > 0$.

$$P_{df2} = \begin{bmatrix} s^* \\ i^* \\ s^*_{\text{ick}} \end{bmatrix} = \begin{bmatrix} \frac{\mu+\gamma}{\mu+\gamma+\omega} \\ 0 \\ 0 \end{bmatrix} \tag{3.6}$$

The local stability of the equilibrium points are determined by the Jacobian matrix shown in Eq. (3.7).

$$J = \begin{bmatrix} -\alpha(1-\theta)i^* - (\mu+\gamma+\omega) & -\alpha(1-\theta)s^* - \gamma & -\gamma \\ \alpha(1-\theta)i^* & \alpha(1-\theta)s^* - (\beta_1+\beta_2+\mu) & 0 \\ 0 & \beta_2 & -(\beta_3+\mu) \end{bmatrix} \tag{3.7}$$

The disease-free equilibrium point P_{df2} is associated with the eigenvalues λ_1, λ_2, and λ_3 in Eqs. (3.8), (3.9), and (3.10), respectively.

$$\lambda_1 = -(\gamma+\mu+\omega); \tag{3.8}$$

$$\lambda_2 = (R_0 - 1)(\beta_1+\beta_2+\mu); \tag{3.9}$$

$$\lambda_3 = -(\beta_3+\mu). \tag{3.10}$$

Theorem 3. *The disease-free EP* $(s^*, i^*, s^*_{ick}) = \left(\frac{\mu+\gamma}{\mu+\gamma+\omega}, 0, 0\right)$ *of the system* (3.1) and (3.2) *is locally asymptotically stable, if* $R_0 < 1$.

Corollary 3.1. *The disease-free EP is locally asymptotically stable, independently of the vaccination rate* ω *and the isolation parameter* θ, *if*

$$\frac{\alpha}{\beta_1+\beta_2+\mu} < 1. \tag{3.11}$$

Proof. It is trivial from the definition of the eigenvalue λ_2 in Eq. (3.9) and R_0 in Eq. (3.5). □

The endemic equilibrium point P_{e2} is provided by Eq. (3.12):

$$P_{e2} = \begin{bmatrix} s^* \\ i^* \\ s^*_{\text{ick}} \end{bmatrix} = \begin{bmatrix} \frac{\beta_1+\beta_2+\mu}{\alpha(1-\theta)} \\ (\beta_3+\mu)\psi \\ \beta_2\psi \end{bmatrix}, \tag{3.12}$$

where

$$\psi = \left(\frac{R_0-1}{R_0}\right)\left(\frac{\gamma+\mu}{(\beta_1+\beta_2+\gamma+\mu)(\beta_3+\mu)+\beta_2\gamma}\right). \tag{3.13}$$

The characteristic equation for the linearization at the endemic EP is given as:

$$\lambda^3 + a_1\lambda^2 + a_2\lambda + a_3 = 0, \tag{3.14}$$

where,

$$\begin{aligned} a_1 &= \psi\alpha(1-\theta)(\beta_3+\mu) + \beta_3 + \gamma + 2\mu + \omega \\ a_2 &= \psi\alpha(1-\theta)((\beta_3+\mu)(\beta_1+\beta_2) + \beta_3(\beta_3+\gamma) \\ &\quad + \mu(3\beta_3+\gamma) + 2\mu^2) + (\beta_3+\mu)(\gamma+\mu+\omega) \\ a_3 &= \psi\alpha(1-\theta)(\beta_3+\mu)(\beta_1\beta_3 + \beta_1\mu + \beta_2\beta_3 + \beta_2\gamma \\ &\quad + \beta_2\mu + \beta_3\gamma \\ &\quad + \beta_3\mu + \gamma\mu + \mu^2), \end{aligned} \tag{3.15}$$

From the Routh–Hurwitz criteria, the polynomial equation (3.14) can be observed to exhibit all roots in the left half-plane, if and only if: (i) a_1, a_2 and a_3 are positive; and, (ii) $a_1a_2 > a_3$.

Theorem 4. *The endemic EP* $(s^*, i^*, s^*_{ick}) = \left(\frac{\beta_1+\beta_2+\mu}{\alpha(1-\theta)}, (\beta_3+\mu)\psi, \beta_2\psi\right)$, *of the systems* (3.1) and (3.2), *exists such that* $(s^*, i^*, s^*_{ick}) \in \mathbb{R}^3_+$, *and is locally asymptotically stable, if* $R_0 > 1$.

Corollary 4.1. *If* $R_0 < 1$, *there is no endemic EP for systems* (3.1) and (3.2), *and the disease dies toward the disease-free EP.*

Proof. To confirm the existence of the endemic EP in $\mathbb{R}^3_+$, it is sufficient to verify that $\psi > 0$, provided that $R_0 > 1$ (see the definition of P_{e2} in Eq. (3.12)), which is trivial, provided the definition of R_0 in (3.5).

In Eq. (3.15), $\psi > 0$ implies $a_i > 0$. To confirm the local stability of endemic EP, we ought to verify $a_1a_2 > a_3$; therefore, the coefficients in Eq. (3.15) can be rewritten as follows:

$$\begin{aligned} a_1 &= \psi p_0 + p_1 \\ a_2 &= \psi p_2 + p_3 \\ a_3 &= \psi p_4, \end{aligned} \tag{3.16}$$

where $p_i > 0$. Subsequently, the second condition in the Routh–Hurwitz criteria becomes:

$$\begin{aligned} (\psi p_0 + p_1)(\psi p_2 + p_3) &> \psi p_4 \\ \psi^2 p_0 p_2 + \psi(p_1 p_2 + p_0 p_3) + p_1 p_3 &> \psi p_4. \end{aligned} \tag{3.17}$$

To verify whether $a_1a_2 > a_3$, at least one of the following conditions ought to be verified to hold:

1. $\psi p_0 p_2 - p_4 > 0$,
2. $p_1 p_2 + p_0 p_3 - p_4 > 0$,
3. $p_1 p_3 - \psi p_4 > 0$.

Expanding the second condition, we obtain:

$$\begin{aligned} \beta_1\beta_3\gamma + \beta_1\beta_3\mu + \beta_1\beta_3\omega + \beta_1\gamma\mu + \beta_1\mu^2 + \beta_1\mu\omega + \\ \beta_2\beta_3\mu + \beta_2\beta_3\omega + \\ \beta_2\mu^2 + \beta_2\mu\omega + \beta_3^3 + 2\beta_3^2\gamma + 5\beta_3^2\mu + 2\beta_3^2\omega + \\ \beta_3\gamma^2 + 6\beta_3\gamma\mu + \\ \beta_3\gamma\omega + 8\beta_3\mu^2 + 5\beta_3\mu\omega + \gamma^2\mu + 4\gamma\mu^2 + \gamma\mu\omega + 4\mu^3 + \\ 3\mu^2\omega > 0, \end{aligned} \tag{3.18}$$

Thus, the existence of the endemic EP in $\mathbb{R}^3_+$ is proved. □

The transcritical bifurcation diagram from the disease-free EP to the endemic EP in the parameter space (θ, ω) for the systems (3.1) and (3.2) is determined by the equation $R_0 = 0$, which gives:

$$\omega = -\left(\frac{\gamma+\mu}{1-\theta_c}\right)\theta + \omega_{\min}, \tag{3.19}$$

where

$$\begin{aligned} \theta_c &= 1 - \left(\frac{\beta_1+\beta_2+\mu}{\alpha}\right), \quad \text{and} \\ \omega_{min} &= \left(\frac{\alpha}{\beta_1+\beta_2+\mu} - 1\right)(\gamma+\mu), \end{aligned} \tag{3.20}$$

provided that $\frac{\alpha}{\beta_1+\beta_2+\mu} > 1$.

The bifurcation diagram is shown in Fig. 3. The dashed blue line signifies the transcritical bifurcation of one of the eigenvalues in each of the equilibrium points, signifying a switch in stability that occurs at $R_0 = 0$. The intersection of the dashed line with the vertical axes represents the minimum vaccination rate required, $\omega_{\min}$, to set a disease-free scenario with no social distancing measures, whereas θ_c represents the critical social distancing measure or any NPI that defines the transition between the disease-free EP to the endemic EP in the absence of vaccines.

The region above the dashed line represents all combinations (θ, ω) that produce stable disease-free EP. The points (θ, ω) below this line produce a stable endemic EP.

According to Eq. (3.12), the closer the pair (θ, ω) is to the origin, the greater the value of the sick (s_{ick}) and the infected (i) populations in the endemic EP.

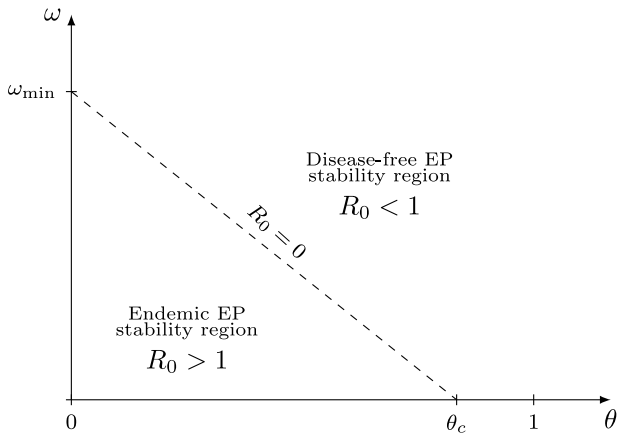

Fig. 3. Bifurcation diagram in the parameter space (θ, ω) for the system (3.1)–(3.2). The dashed line illustrated in the diagram corresponds to the condition $R_0 = 0$ in Eq. (3.9), which demarcates the boundary between the disease-free equilibrium point and the endemic equilibrium point. This representation provides insights into the system's stability and the impact of changes in the parameters on the dynamics of the system.

4. Parametric SIRSi-Vaccine model fitting

To test the results from Section, the parameters of the SIRSi model in Eq. (2.6) were determined numerically through parametric fitting using publicly available data of one of the larger cities of Brazil, the city of São Paulo [67]. The aim of the fitting was not necessarily to facilitate Covid-19 pandemic predictions, however to analyze possible scenarios considering variations in two of the most relevant variables in any epidemiological model: the transmission and vaccination rates.

The data collected correspond to the confirmed cases of Covid-19 during May 2020, for the fitting (from 2020-04-30 to 2020-05-30) and the subsequent month (from 2020-05-30 to 2020-06-30) for validation [68]. According to the data source, during the mentioned period, a reported Covid-19 case was confirmed by the following criteria: (i) a positive RT-PCR[2] test result performed by an authorized laboratory according to the Brazilian Health Authority; or (ii) clinical and epidemiological criteria, that is, reported close contact with a confirmed case of Covid-19 in the 14 days prior to symptom onset.

The SIRSi-Vaccine model considers the effect of social distancing on the Covid-19 infectiousness. Previous studies that the Covid-19 epidemiological models are strongly sensitive to this parameter [33,69–71]. The data used to model social distancing were obtained from privacy-protected mobile phone location information [72] corresponding to May 2020, provided by mobile phone carries.

The social distancing index time history is shown in Fig. 4 for the year 2020. It can be observed that the series is time-varying, presenting a small-amplitude oscillatory behavior around a constant value, with a short period of approximately 7 days (see [72]), and a long period of approximately 6 months.

Based on Fig. 4, the social distancing dynamics could be modeled as an impulse-driven oscillator; however, to maintain the mathematical reasoning as simple as possible, and to preserve both the analytical and the numerical insights, a first-order polynomial equation was selected to model the behavioral trend observed in the data during the period considered. The first-order social distancing index polynomial fitting is shown in Fig. 5. Using the least-square fitting method, we obtained the following approximation:

$$\theta(t) = a_1 t + a_0, \tag{4.1}$$

provided that $a_1 = 2.6 \times 10^{-4}$ and $a_0 = 0.5$. This approximation was based on the isolation index data corresponding to May 2020, and contains a root-mean-square error (RMSE) of 0.169; the data and the linear approximation are shown in Fig. 5. The time-series in Fig. 4 shows that the lower and upper bounds for the isolation index data during this period were 0.35 and 0.6, respectively.

Nevertheless, the oscillatory behavior of the social distancing index is not completely disregarded, as in Section 5, a simulation result for an oscillatory social distancing index is shown.

We used the least-squares trust region reflective (TRR) algorithm [73,74], which is a robust real-time optimization method, fitting the s_{ick} population in Eq. (2.6) to the number of confirmed Covid-19 cases. The root-mean-square error (RMSE) for this fitting was 7.3×10^{-5}. The approximation presented was derived from data that has been normalized against the total population reported by [68] for May 2020.

The free parameters in the fitting process are α, γ, β_1, β_2, β_3, and i_0 (Fig. 2). For the initial condition, s_{ick0} was considered as the normalized first data sample from the confirmed cases time-series; the initial number of infected/infectious population i_0 was considered as a random value with lower and upper bounds equal to one and three times the number of confirmed cases, respectively, as reported by Lima et al. and Sansone et al. [75,76]; the initial value for the recovered population r_0 was set to 90% of the initial sick population [77,78]; the initial susceptible population s_0 was computed as $s(t) = 1 - i(t) - s_{\text{ick}}(t) - r(t)$. For the initial guess in the fitting process, bounded random values were considered for each free parameter.

To validate the predictions generated by the model with adjusted parameters, the data on confirmed cases for the month of June 2020, normalized with respect to the total population, was used. The root mean square error (RMSE) was calculated to be 1.06×10^{-4}. Fig. 6 presents the simulation results.The fitting results are shown in Table 1.

Fig. 6 shows the trajectory of the S_{ick} population after the fitting process separately with the fitting and the validation data.

5. Simulation results

Hypothetical scenarios were analyzed from the SIRSi-Vaccine model in Eqs. (3.1) and (3.2), with parameters fitted in Section 4, for different values of isolation index and vaccination rate.

The bifurcation diagram shown in Fig. 3 can now be modified with the set of fitted parameters in Table 1, and is shown by the dashed line in Fig. 11. The intersections of the line $R_0 = 0$, that is, $\omega_{\text{min}} = 0.028$ and $\theta_c = 0.58$, suggest that at the considered disease stage shown in Fig. 6, the epidemic could have been controlled with NPI (non-pharmacologic intervention) separately, including distancing measures at values > 0.58, implemented for at least 24 months.

The number of confirmed cases for this scenario is shown in Fig. 7 (for $\theta = 0.59$), where a maximum peak of 21,000 confirmed cases out of 12 million people would be attained in July 2020. It is important to note that from the historical series of the isolation index in Fig. 4, the maximum isolation index recorded in 2020 was approximately 0.59 at the beginning of the pandemic, and the lowest isolation index was 0.25 before any NPI

[2] Reverse Transcription-Polymerase Chain Reaction.

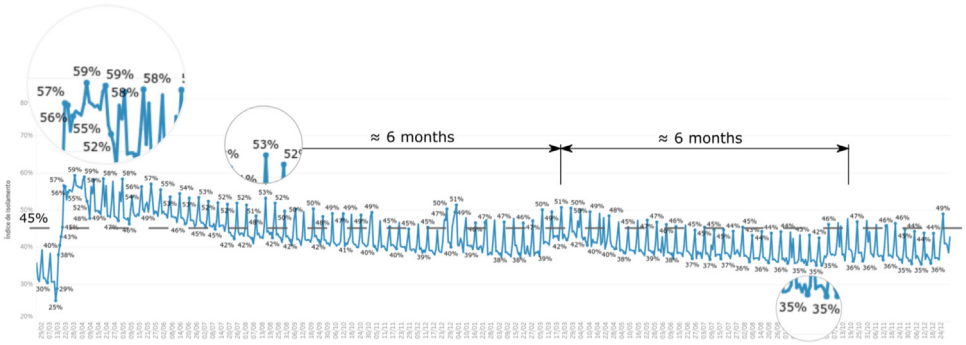

Fig. 4. Temporal trend of the Isolation Index in São Paulothroughout 2020, as derived from publicly available data provided by SEADE (Foundation of the Data Analysis System of the State of São Paulo), as reported by [72]. The vertical axis shows the isolation index as a percentage, whereas the horizontal axis displays the data (in day/month format), during sampling. The Isolation Index peaked at 59% in March 2020 during the initial phase of the pandemic, and declined to its lowest point of 35% in September of the same year.

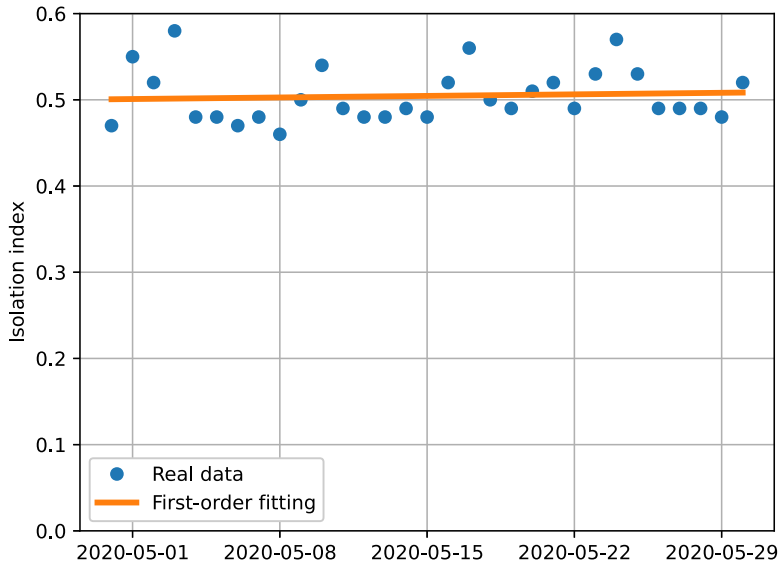

Fig. 5. Isolation index data for May 2020, together with the linear approximation obtained through fitting. The linear approximation, as depicted in Eq. (4.1) represents the best-fit line that characterizes the relationship between the isolation index and time. It also provides a simplified model for understanding the temporal trends in the isolation index.

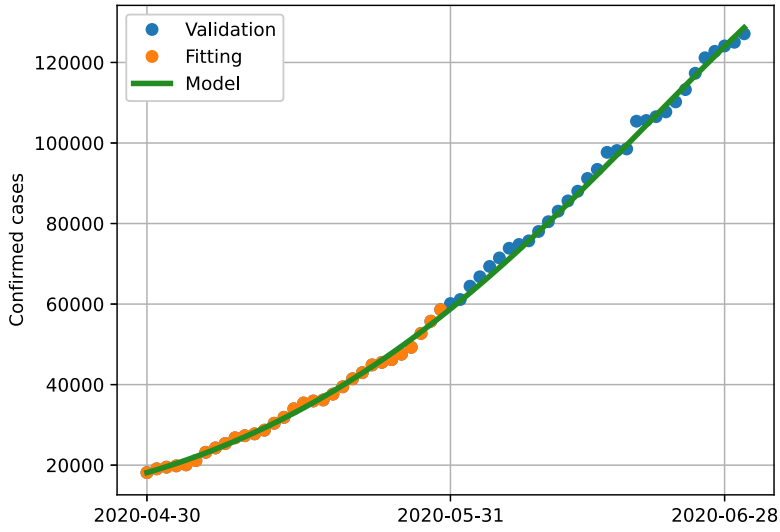

Fig. 6. Data used for parameter fitting and validation, together with the corresponding prediction curve. The orange circles represent the data used for fitting the model parameters, whereas the blue circles represent the validation data. The solid line shows the predicted values generated by the fitted model (2.6). The root-mean-square error (RMSE) for the validation data is 1.06×10^{-4}. (For interpretation of the references to color in this figure legend, the reader is referred to the web version of this article.)

Table 1
Summary of the parameters for the SIRSi model as specified in Eq. (2.4). The table includes the reported maximum and minimum values for each parameter based on the literature, and the estimated values obtained through fitting.

	Description	Min. & Max. values	Parameter value	Refs.
N	Total population in the city of São Paulo in model (2.2).		11,869,660	[33,68,79]
μ	Daily birth and death rate in model (2.4).		3.5945×10^{-5}	[33,80]
α	Transmission rate.	[0.24; 1.00]	0.52[a]	[33,81,82]
θ	Social distancing index.	[0; 1]	$a_1 t + a_0$[a]	[33,72]
γ	Immunity loss rate.	[0.0067; 0.02]	0.02[a]	[83–85]
β_1	Recovery rate for asymptomatic.	[0.1; 0.2]	0.1[a]	[86,87]
β_2	Symptom onset rate.	[0.1; 0.3]	0.11[a]	[33,87]
β_3	Recovery rate for symptomatic.	[0.07; 0.2]	0.13[a]	[82,84]
s_0	Susceptible initial condition	$s(t)=1-i(t)-s_{\text{ick}}(t)-r(t)$	0.996[a]	
i_0	Infected/infectious initial condition	$[1; 3] \times s_{\text{ick0}}$	0.0022[a]	[75,76]
s_{ick0}	Confirmed cases initial condition	Collected from the normalized initial date	0.0015	

[a]Fitted.

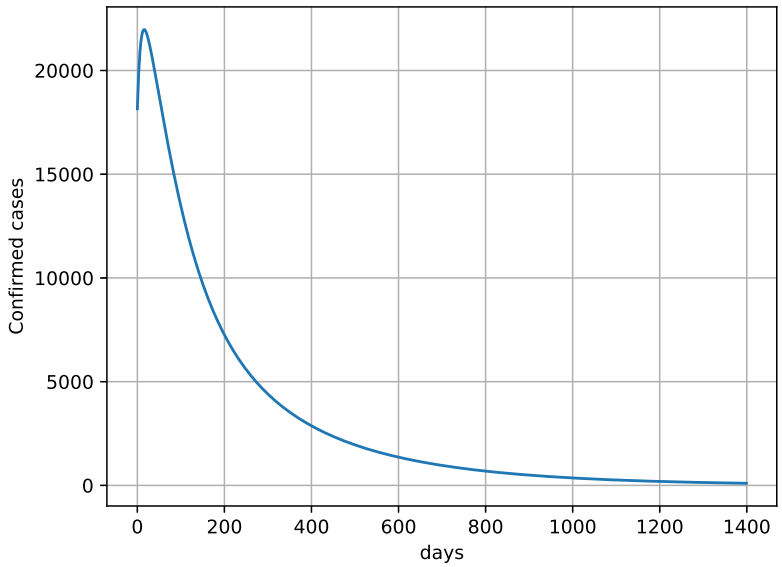

Fig. 7. Illustration of the confirmed cases curve over time, with a fixed isolation index of 0.59, which is close to the critical value $\theta_c = 0.58$ (as shown in Fig. 11), in the absence of vaccination. The data indicates that implementing effective isolation measures could potentially eradicate the pandemic, even in the absence of a vaccination strategy, despite extended periods of isolation.

measure. Therefore, isolation index equivalent to 0.59 could be theoretically possible. However, an NPI as high as 59% maintained for such a long time as to end the pandemic, would collaterally produce high economic losses, which is equally undesirable.

Fig. 8 shows another hypothetical scenario in the opposite end of the bifurcation diagram, where without any NPI ($\theta = 0$), vaccination rate is considered separately close to $\omega_{\min} = 0.028$ within the disease-free region. The percentage of vaccinated per day, provided by the product $\omega s(t)$, starts at 3% and it decreases to approximately 1% of the population per day, while approaching the pandemic end. In this hypothetical case, although the disease-free EP can be attained, the number of confirmed cases exceeds half a million in less than a month after the beginning of the data collection, representing over twenty times that of the number of confirmed cases in the previous scenario.

The isolation index historical series (Fig. 4) presents an oscillatory behavior—the first month of data collection can be considered as transient. This time-series can be approximated as a two-frequency small-amplitude oscillation signal around a constant value θ_m:

$$\theta(t) = \theta_m + A_1 \sin(2\pi t/T_1) + A_2 \sin(2\pi t/T_2), \tag{5.1}$$

and from Fig. 4, $\theta_m = 0.45$, $A_1 = 0.05$, $T_1 = 7$ days, $A_2 = 0.075$, and $T_2 = 6 \times 30$ days. This seasonal oscillation, with two periods:

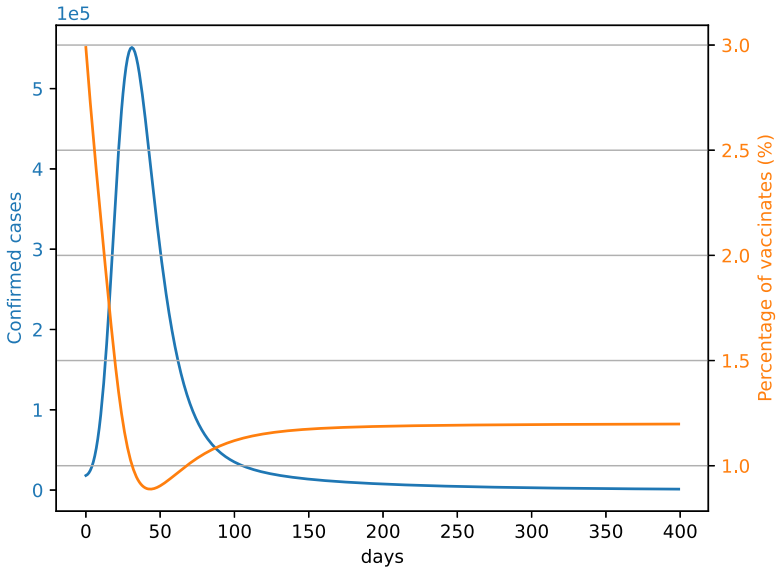

Fig. 8. Illustration of two curves with a fixed vaccination rate of 0.03, proximate to $\omega_{\min} = 0.028$, representing the minimum vaccination threshold required to preserve the stable disease-free equilibrium in the absence of NPI measures (Fig. 11). The first curve portrays the confirmed cases over time, showing a sharp peak in the second month of the pandemic. The second curve exhibits the percentage of vaccinated population, initiated at 3% and progressively declining to below half after 6 months.

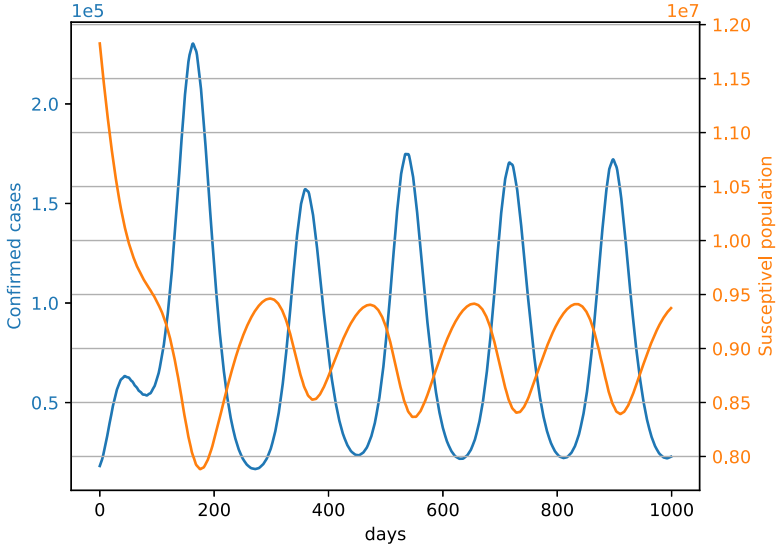

Fig. 9. Two periodic curves with a constant vaccination rate of 0.04. The isolation index was modeled as a two-period series, comprising a short 7 days period and a long 6 months period, as illustrated in Eq. (5.1). The first curve represents the confirmed cases over time ($S_{\text{ick}}(t)$), showing sharp peaks every 6 months. The second curve portrays the susceptible population ($S(t)$), which oscillates with the same frequency, however with an estimated 2 months delay.

the short period of 7 days and the long period of 6 months could result in constant oscillations obtained from Eqs. (3.1) and (3.2).

Simulations of this scenario, with $\omega = 0.04$ are shown in Figs. 9 and 10. Trajectories of $S_{\text{ick}}(t)$ and $S(t)$ suggest that the 6 months small-variations in the isolation index can force the steady high-amplitude 6 months oscillations in the number of confirmed cases. The recognition of seasonal patterns in airborne diseases have been studied extensively in the literature, although the underlying mechanisms remain poorly understood [88]. This hypothetical scenario was only intended to highlight the possibility of successive waves of confirmed cases caused by small variations in the isolation index and variations that could be a consequence of the relaxation of security measures such as the use of masks in public places.

Fig. 11 shows the contours of the peaks of the confirmed cases in percentages of the total population, in the parameter space (θ, ω), with all other parameters as shown in previous section. The contours show that the closer the (θ, ω) pair is to the origin, the higher the peak of confirmed cases. Furthermore, the increase of NPI – the isolation index in this case – reduces the peak of confirmed cases, even in the endemic region. On the other hand, lower isolation values lead to higher peaks in the number of confirmed cases, even within the disease-free region.

6. Discussions and limitations of the SIRSi-Vaccine model

The model contains limitations when considering the validation data, as the values of the parameters obtained by the fit, as shown in Fig. 6. The simulations were performed considering hypothetical scenarios.

Qualitatively, confirmed cases show a decrease after 2 years, adopting strict isolation measures, close to 58% and without any

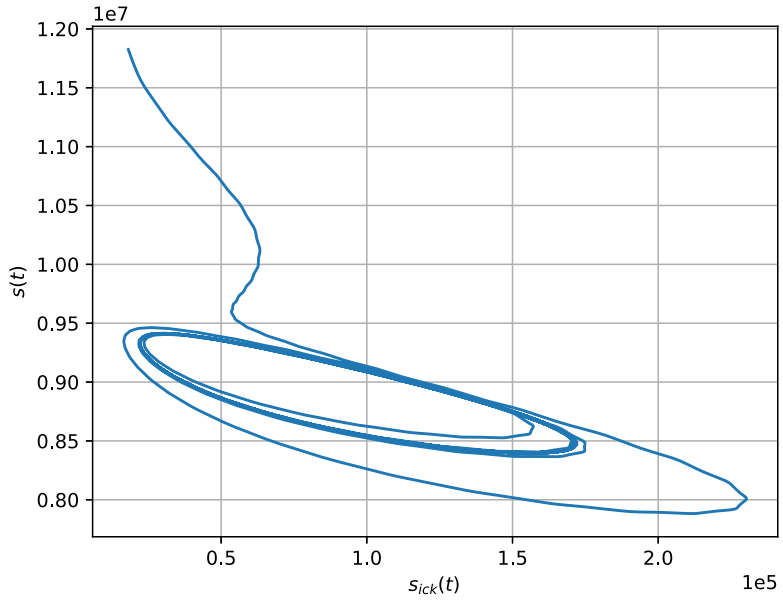

Fig. 10. Phase plot representing the trajectories of confirmed cases ($S_{\text{ick}}(t)$) and susceptible population ($S(t)$). The curves were generated with a constant vaccination rate of 0.04, whereas the isolation index was modeled as a two-period series as depicted in Eq. (5.1). The periodic orbit of the solution is shown, highlighting the cyclical nature of the pandemic dynamics under the given conditions.

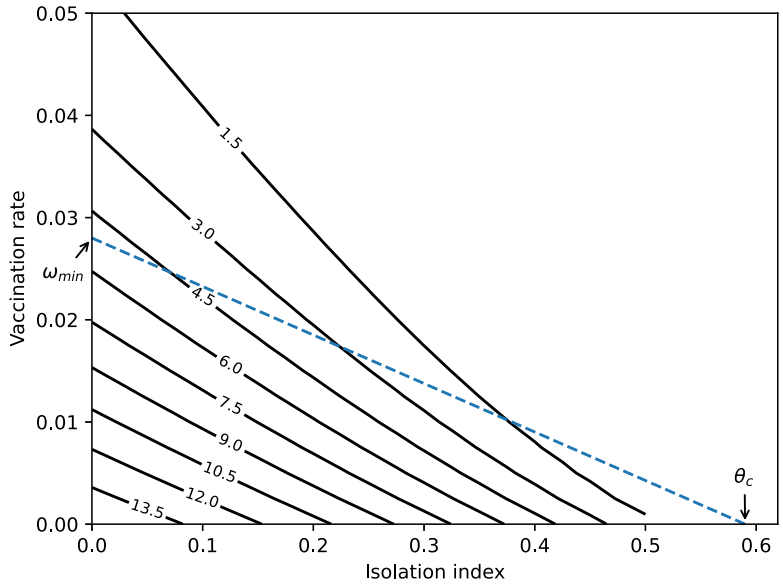

Fig. 11. Contour graph displayed in a dark solid line representing the peaks of confirmed cases ($S_{\text{ick}}(t) \times 10^5$) as a percentage of the total population. These contours are shown as a function of the vaccination rate (ω) and the isolation index (θ). In addition, the bifurcation curve for $R_0 = 0$ represented in Eq. (3.5), is shown in dashed blue line; the intersection of this curve with the axes indicates the critical value for the isolation index ($\theta_c = 0.58$) and minimum vaccination rate ($\omega_{\text{min}} = 0.028$). This curve further establishes the boundaries between the stable regions for the endemic equilibrium point and the disease-free equilibrium point, as previously illustrated in Fig. 3.

vaccine, indicating the infeasibility of the cost for such measures, considering the city of São Paulo as the object of study (Fig. 7).

With the introduction of the vaccine and considering the minimum vaccination effort $\omega_{min} \approx 0.03$, the number of vaccinated would be $\omega S(t)$ per day; considering that even in this hypothetical situation, the number of confirmed cases would remain considerably high, the period for the extinction of the disease would be close to three months (Fig. 8).

In practical application, the observed situations were not limited to the consideration of either vaccination or isolation measures separately. Rather, there were potential scenarios, in which the combination of both interventions may effectively mitigate the spread of the disease. Fig. 11 illustrates the combination of two such effective interventions: social isolation and vaccination. The bifurcation diagram in this Fig. 11 represents a qualitative change in the model's behavior. The region below the dashed line indicates the region of endemic equilibrium stability, whereas the region above this line is considered the disease-free region, which is stable.

In the endemic region of the bifurcation graph, below the dashed blue line in Fig. 11, all combinations of isolation and vaccination parameters imply that the disease will persist within the population, even with significant efforts in vaccination and preventive NPI measures. The numerical values shown along each black curve represents the peak of the confirmed cases. As depicted in Fig. 11, the incidence of infection peaks can be mitigated

through two approaches: augmenting the vaccination rate or elevating the isolation rate. However, the complete elimination of the disease can only be accomplished when the parameter values are located within the region above the bifurcation curve, which corresponds to the stable disease-free equilibrium point.

From the historical series indicated in Fig. 4, it can be observed that the isolation rate was not constant, however periodic. Periodicity was observed in the isolation index of 7 days and 6 months.

For the simulations, the two periods, 7 days and 6 months were considered, shown in Figs. 9 and 10. The trajectories shown in Fig. 9, calculated with $\omega = 0.04$, which is in the disease-free region, suggest that the small-amplitude oscillation in θ can force an oscillatory behavior in the system, breaking the equilibrium point to produce a stable limit-cycle that can be observed in the phase portrait. Fig. 10 shows the limit cycle that relates the number of confirmed and susceptible infected individuals, produced by the variation of the isolation index. Semiannual variations in the the isolation rate can produce significant oscillations of the same frequency in the number of infected.

The models presented in the first sections exhibit two distinct equilibrium points, which were mutually exclusive. Notably, a transcritical bifurcation appears because of the sign change in one of the eigenvalues, when the parameters vary (Figs. 3 and 11). Interestingly, these models do not demonstrate Hopf bifurcations, and consequently, do not allow for the identification of natural periodic solutions.

Notwithstanding, under the influence of a periodic isolation index with a small amplitude and a period of 6 months, the system exhibits forced periodic solutions with a similar period and high amplitude, comparable to the peaks of the undisturbed response, as shown in Fig. 9. This small-amplitude periodic fluctuation in the isolation index is evident in the historical data, as depicted in Fig. 4.

This implies that a SIRSi model with vaccine subjected to a forced term can yield other periodic solutions. The forced terms can encompass variations in seasonal parameters, which have been demonstrated to exert a significant influence. However, a comprehensive analysis of these effects necessitates a fresh approach to the problem, which is beyond the scope of this study. Nevertheless, we aim to investigate these challenges in our future work.

7. Conclusions

This work presents a novel compartmental model for Covid-19 that estimates the number of unreported infected individuals by accounting for the confirmed cases, vaccination rates, and social distancing index. The model sheds light on the dynamics of the disease and its impact on the spread of Covid-19. Additionally, we analyzed the conditions for the local stability in both disease-free and endemic equilibrium, which provides insights into the behavior of the disease in different scenarios.

The model aimed to show the variation of certain parameters and their influence on the qualitative responses associated with the dynamics of virus propagation. From the analysis of the model, the possibility of the existence of two equilibrium points (disease-free and endemic) was verified.

With the introduction of vaccination associated with social isolation, we concluded that there is a minimum effort in vaccination and social isolation that ensures the existence of equilibrium points.

For the disease-free point, the transcritical bifurcation condition suggests that there is a possibility for the propagation dynamics to become endemic. Furthermore, for the endemic point, the existence condition guarantees that if it exists, it is stable. Moreover, as the disease-free and endemic equilibrium points do not occur simultaneously, in both cases, local stability implies global stability [51].

The analysis of the conditions for the local stability model and the transcritical bifurcation diagram in the parameter space (θ, ω) provides valuable insights into the behavior of the disease in different scenarios. In Section 5, the possibility of forced limit cycles owing to small-amplitude oscillations in the isolation index is shown, which may help explain the periodicity of the waves of infection. This observation suggests that further research is required to better understand the dynamics of Covid-19 and develop effective strategies for controlling the disease.

The transcritical bifurcation diagram was used to study the influence of the isolation index and vaccination rate on the switching stability between the endemic and disease-free equilibrium. The diagram also shows the contours of the maximum number of infected in the same parameter space, which helps policymakers to understand the impact of different interventions on the spread of the disease.

Investigating the spread of Covid-19 in the city of São Paulo includes the consideration of the socio-demographic differences of the most populous city in the country. For a detailed analysis of viral dissemination, it is essential to account for the differences in education, regional occupation, income, and access to health services; and to summarize the economic, environmental, and social conditions of the population residing in the region.

As the data considered for model validation includes the population of the entire city homogeneously, the simulations showed that based on the periodicity of social distancing index, there is a limit cycle, indicating that preventive measures such as social isolation combined with vaccination may not ensure a disease-free equilibrium [89], yielding different responses when considering socio-demographic specifications.

Considering a vaccination rate higher than the minimum necessary, and even considering the combination of parameters that ensure disease-free points, the periodicity of contagions was verified, considering the peaks of infection, suggesting the necessity for understanding the phenomenon.

In conclusion, this study contributes to the ongoing efforts to understand the dynamics of Covid-19 and control its spread. The novel compartmental model proposed in this study provides a framework for estimating the number of unreported infected individuals, which is crucial for developing effective strategies for controlling the disease.

Declaration of competing interest

The authors declare that they have no known competing financial interests or personal relationships that could have appeared to influence the work reported in this paper.

Data availability

Data used in this study are publicly available [61,72]. All datasets used in this work, together with the code for the simulations, are available at (https://github.com/dferruzzo/Covid-19.git).

References

[1] Maxmen A. Why did the world's pandemic warning system fail when COVID hit? Nature 2021;589:499–500. http://dx.doi.org/10.1038/d41586-021-00162-4.

[2] World Health Organization. Archived: WHO timeline - COVID-19. 2020, https://www.who.int/news-room/detail/27-04-2020-who-timeline---COVID-19. [Accessed 25 June 2020].

[3] Repurposed antiviral drugs for COVID-19 — Interim WHO solidarity trial results. N Engl J Med 2021;384(6):497–511. http://dx.doi.org/10.1056/NEJMoa2023184.
[4] Johnston C, Brown ER, Stewart J, Karita HC, Kissinger PJ, Dwyer J, et al. Hydroxychloroquine with or without azithromycin for treatment of early SARS-CoV-2 infection among high-risk outpatient adults: A randomized clinical trial. EClinicalMedicine 2021;33(100773). http://dx.doi.org/10.1016/j.eclinm.2021.100773.
[5] Tomlinson B, Eftekhar SP, Kazemi S, Barary M, Javanian M, Ebrahimpour S, et al. Effect of hydroxychloroquine and azithromycin on qt interval prolongation and other cardiac arrhythmias in COVID-19 Confirmed Patients. Cardiovasc Ther 2021;20021(6683098). http://dx.doi.org/10.1155/2021/6683098.
[6] Bush LM, Rahman AK, Purdy AG, Ender PT. COVID-19 pneumonia in patients on chronic hydroxychloroquine therapy: Three cases of COVID-19 pneumonia. Case Rep Infect Dis 2020;2020(8822753). http://dx.doi.org/10.1155/2020/8822753.
[7] Bignardi PR, Vengrus CS, Aquino BM, Neto AC. Use of hydroxychloroquine and chloroquine in patients with COVID-19: a meta-analysis of randomized clinical trials. Pathog Glob Health 2021;115(3):1–12. http://dx.doi.org/10.1080/20477724.2021.1884807.
[8] Chu DK, Akl EA, Duda S, Solo K, Yaacoub S, Schünemann HJ, et al. Physical distancing, face masks, and eye protection to prevent person-to-person transmission of SARS-CoV-2 and COVID-19: a systematic review and meta-analysis. Lancet 2020;395(10242):1973–87. http://dx.doi.org/10.1016/S0140-6736(2031142-9).
[9] de Souza Santos AA, Candido DdS, de Souza WM, Buss L, Li SL, Pereira RHM, et al. Dataset on SARS-CoV-2 non-pharmaceutical interventions in Brazilian municipalities. Sci Data 2021;8(1):73. http://dx.doi.org/10.1038/s41597-021-00859-1.
[10] Scheid JL, Lupien SP, Ford GS, West SL. Commentary: Physiological and psychological impact of face mask usage during the COVID-19 pandemic. Int J Environ Res Public Health 2020;17(18):6655. http://dx.doi.org/10.3390/ijerph17186655.
[11] Miguel-Arribas A, Aleta A, Moreno Y. Impact of vaccine hesitancy on secondary COVID-19 outbreaks in the US: an age-structured SIR model. BMC Infect Dis 2022;22(1):511. http://dx.doi.org/10.1186/s12879-022-07486-0.
[12] Ministério da Saúde do Brasil. In: Painel coronavírus. 2020, https://covid.saude.gov.br. [Accessed 28 March 2020].
[13] Ball P. The lightning-fast quest for COVID vaccines - and what it means for other diseases. Nature 2021;589(7840):16–8. http://dx.doi.org/10.1038/d41586-020-03626-1.
[14] Wolf J, Bruno S, Eichberg M, Jannat R, Rudo S, VanRheenen S, et al. Applying lessons from the Ebola vaccine experience for SARS-CoV-2 and other epidemic pathogens. Npj Vacc 2020;5(1):51. http://dx.doi.org/10.1038/s41541-020-0204-7.
[15] Finnegan G. Vaccines today. In: Ebola vaccine success shows how to beat COVID-19. 2021, https://www.vaccinestoday.eu/stories/ebola-vaccine-success-shows-how-to-beat-covid-19/. [Accessed 15 February 2021].
[16] Zimmer C, Corum J, Wee SL. The New York times. In: Coronavirus vaccine tracker. 2022, https://www.nytimes.com/interactive/2020/science/coronavirus-vaccine-tracker.html. [Accessed 31 August 2022].
[17] Cancian N, Machado R, de São Paulo Folha. Por unanimidade. In: Anvisa aprova uso emergencial de vacinas contra COVID-19. 2021, https://folha.com/zvx62qr8. [Accessed 20 March 2021].
[18] Dagan N, Barda N, Kepten E, Miron O, Perchik S, Katz MA, et al. BNT162b2 mRNA COVID-19 vaccine in a nationwide mass vaccination setting. N Engl J Med 2021;384(15):1412–23. http://dx.doi.org/10.1056/NEJMoa2101765.
[19] Ritchie H, Ortiz-Ospina E, Beltekian D, Mathieu E, Hasell J, Macdonald B, et al. Our world in data. In: Coronavirus (COVID-19) vaccinations. 2021, https://ourworldindata.org/covid-vaccinations. [Accessed 22 March 2021].
[20] Estadilla CDS, Uyheng J, de Lara-Tuprio EP, Teng TR, Macalalag JMR, Estuar MRJE. Impact of vaccine supplies and delays on optimal control of the COVID-19 pandemic: mapping interventions for the Philippines. Infect Dis Poverty 2021;10(1):107. http://dx.doi.org/10.1186/s40249-021-00886-5.
[21] Moore JP, Offit PA. SARS-CoV-2 Vaccines and the growing threat of viral variants. JAMA 2021;325(9):821–2. http://dx.doi.org/10.1001/jama.2021.1114.
[22] Kadire SR, Wachter RM, Lurie N. Delayed second dose versus standard regimen for COVID-19 vaccination. N Engl J Med 2021;384(9):28. http://dx.doi.org/10.1056/NEJMclde2101987.
[23] Bartsch SM, O'Shea KJ, Ferguson MC, Bottazzi ME, Wedlock PT, Strych U, et al. Vaccine efficacy needed for a Covid-19 coronavirus vaccine to prevent or stop an epidemic as the sole intervention. Am J Prev Med 2020;59(4):493–503. http://dx.doi.org/10.1016/j.amepre.2020.06.011.
[24] Tolles J, Luong T. Modeling epidemics with compartmental models. JAMA 2020;323(24):2515–6. http://dx.doi.org/10.1001/jama.2020.8420.
[25] Jewell NP, Lewnard JA, Jewell BL. Predictive mathematical models of the COVID-19 pandemic: Underlying principles and value of projections. JAMA 2020;323(19):1893–4. http://dx.doi.org/10.1001/jama.2020.6585.
[26] ArunKumar K, Kalaga DV, Sai Kumar CM, Chilkoor G, Kawaji M, Brenza TM. Forecasting the dynamics of cumulative COVID-19 cases (confirmed, recovered and deaths) for top-16 countries using statistical machine learning models: Auto-regressive integrated moving average (ARIMA) and seasonal auto-regressive integrated moving average (SARIMA). Appl Soft Comput 2021;103:107161. http://dx.doi.org/10.1016/j.asoc.2021.107161.
[27] Fiacchini M, Alamir M. The Ockham's Razor applied to COVID-19 model fitting French data. Annu Rev Control 2021;51:500–10. http://dx.doi.org/10.1016/j.arcontrol.2021.01.002.
[28] Markovič R, Šterk M, Marhl M, Perc M, Gosak M. Socio-demographic and health factors drive the epidemic progression and should guide vaccination strategies for best COVID-19 containment. Results Phys 2021;26:104433. http://dx.doi.org/10.1016/j.rinp.2021.104433.
[29] Piraveenan M, Sawleshwarkar S, Walsh M, Zablotska I, Bhattacharyya S, Farooqui HH, et al. Optimal governance and implementation of vaccination programmes to contain the COVID-19 pandemic. R Soc Open Sci 2021;8(6):210429. http://dx.doi.org/10.1098/rsos.210429.
[30] Tchoumi S, Diagne M, Rwezaura H, Tchuenche J. Malaria and COVID-19 co-dynamics: A mathematical model and optimal control. Appl Math Model 2021;99:294–327. http://dx.doi.org/10.1016/j.apm.2021.06.016.
[31] Alenezi MN, Al-Anzi FS, Alabdulrazzaq H. Building a sensible SIR estimation model for COVID-19 outspread in Kuwait. Alex Eng J 2021;60(3):3161–75. http://dx.doi.org/10.1016/j.aej.2021.01.025.
[32] Muñoz-Fernández GA, Seoane JM, Seoane-Sepúlveda JB. A SIR-type model describing the successive waves of COVID-19. Chaos Solitons Fractals 2021;144:110682. http://dx.doi.org/10.1016/j.chaos.2021.110682.
[33] Batistela CM, Correa DP, Bueno AM, Piqueira JRC. SIRSi compartmental model for COVID-19 pandemic with immunity loss. Chaos, Solitons Fractals 2021;142:110388. http://dx.doi.org/10.1016/j.chaos.2020.110388.
[34] Zhai S, Du M, Wang Y, Liu P. Effects of heterogeneous susceptibility on epidemiological models of reinfection. Nonlinear Dynam 2023;111(2):1891–902. http://dx.doi.org/10.1007/s11071-022-07870-0.
[35] Nakamura G, Grammaticos B, Deroulers C, Badoual M. Effective epidemic model for COVID-19 using accumulated deaths. Chaos Solitons Fractals 2021;144:110667. http://dx.doi.org/10.1016/j.chaos.2021.110667.
[36] Wei W, Duan B, Zuo M, Zhu Q. An extended state observer-based U-model control of the COVID-19. ISA Trans 2021;124:115–23. http://dx.doi.org/10.1016/j.isatra.2021.02.039.
[37] Morato MM, Pataro IM, Americano da Costa MV, Normey-Rico JE. A parametrized nonlinear predictive control strategy for relaxing COVID-19 social distancing measures in Brazil. ISA Trans 2022;124:197–214. http://dx.doi.org/10.1016/j.isatra.2020.12.012.
[38] Ma W, Zhao Y, Guo L, Chen Y. Qualitative and quantitative analysis of the COVID-19 pandemic by a two-side fractional-order compartmental model. ISA Trans 2022;124:144–56. http://dx.doi.org/10.1016/j.isatra.2022.01.008.
[39] Kumar N, Kumar H. A novel hybrid fuzzy time series model for prediction of COVID-19 infected cases and deaths in India. ISA Trans 2022;124:69–81. http://dx.doi.org/10.1016/j.isatra.2021.07.003.
[40] Gupta M, Jain R, Taneja S, Chaudhary G, Khari M, Verdú E. Real-time measurement of the uncertain epidemiological appearances of COVID-19 infections. Appl Soft Comput 2021;101:107039. http://dx.doi.org/10.1016/j.asoc.2020.107039.
[41] Blyuss K, Kafieh R, Arian R, Saeedizadeh N, Amini Z, Serej ND, et al. COVID-19 in Iran: Forecasting pandemic using deep learning. Comput Math Methods Med 2021;2021:6927985. http://dx.doi.org/10.1155/2021/6927985.
[42] Angeli M, Neofotistos G, Mattheakis M, Kaxiras E. Modeling the effect of the vaccination campaign on the COVID-19 pandemic. Chaos Solitons Fractals 2022;154:111621. http://dx.doi.org/10.1016/j.chaos.2021.111621.
[43] Li T, Guo Y. Modeling and optimal control of mutated COVID-19 (delta strain) with imperfect vaccination. Chaos Solitons Fractals 2022;156:111825. http://dx.doi.org/10.1016/j.chaos.2022.111825.
[44] de León UAP, Avila-Vales E, Lin Huang K. Modeling COVID-19 dynamic using a two-strain model with vaccination. Chaos, Solitons Fractals 2022;157:111927. http://dx.doi.org/10.1016/j.chaos.2022.111927.
[45] Luo G, Zhai S, Zhou P, Tao J. A bi-virus competing model with time-varying susceptibility and repeated infection. Nonlinear Anal RWA 2022;67:103636. http://dx.doi.org/10.1016/j.nonrwa.2022.103636.
[46] Yasuda H, Ito F, Hanaki KI, Suzuki K. Covid-19 pandemic vaccination strategies of early 2021 based on behavioral differences between residents of Tokyo and Osaka, Japan. Arch Public Health 2022;80(1):180. http://dx.doi.org/10.1186/s13690-022-00933-z.
[47] Broeck WVD, Gioannini C, Gonçalves B, Quaggiotto M, Colizza V, Vespignani A. The GLEaMviz computational tool, a publicly available software to explore realistic epidemic spreading scenarios at the global scale. BMC Infect Dis 2011;11(1):37. http://dx.doi.org/10.1186/1471-2334-11-37.
[48] Zhai S, Luo G, Huang T, Wang X, Tao J, Zhou P. Vaccination control of an epidemic model with time delay and its application to COVID-19. Nonlinear Dynam 2021;106(2):1279–92. http://dx.doi.org/10.1007/s11071-021-06533-w.

[49] Zhai S, Gao H, Luo G, Tao J. Control of a multigroup COVID-19 model with immunity: treatment and test elimination. Nonlinear Dynam 2021;106(2):1133–47. http://dx.doi.org/10.1007/s11071-020-05961-4.
[50] Andronov AA. Qualitative theory of second-order dynamic systems. Halsted Press; 1973.
[51] Guckenheimer J, Holmes P. Nonlinear oscillations, dynamical systems, and bifurcations of vector fields. Springer Science & Business Media; 2013.
[52] Helbing D, Brockmann D, Chadefaux T, Donnay K, Blanke U, Woolley-Meza O, et al. Saving human lives: What complexity science and information systems can contribute. J Stat Phys 2015;158(3):735–81. http://dx.doi.org/10.1007/s10955-014-1024-9.
[53] Zou L, Ruan F, Huang M, Liang L, Huang H, Hong Z, et al. SARS-CoV-2 viral load in upper respiratory specimens of infected patients. N Engl J Med 2020;382(12):1177–9. http://dx.doi.org/10.1056/NEJMc2001737.
[54] Zhang J, Tian S, Lou J, Chen Y. Familial cluster of COVID-19 infection from an asymptomatic. Crit Care 2020;24(1):7–9. http://dx.doi.org/10.1186/s13054-020-2817-7.
[55] Tian S, Hu N, Lou J, Chen K, Kang X, Xiang Z, et al. Characteristics of COVID-19 infections in Beijing. J Infect 2020;80(4):401–6. http://dx.doi.org/10.1016/j.jinf.2020.02.018.
[56] Feng S, Feng Z, Ling C, Chang C, Feng Z. Prediction of the COVID-19 epidemic trends based on SEIR and AI models. PLoS One 2021;16(1):e0245101. http://dx.doi.org/10.1371/journal.pone.0245101.
[57] Godio A, Pace F, Vergnano A. SEIR modeling of the Italian epidemic of SARS-CoV-2 using the computational swarm intelligence. Int J Environ Res Public Health 2020;17:3535. http://dx.doi.org/10.20944/preprints202004.0073.v1.
[58] Kellam P, Barclay W. The dynamics of humoral immune responses following SARS-CoV-2 infection and the potential for reinfection. J Gen Virol 2020;101(8):791–7. http://dx.doi.org/10.1099/jgv.0.001439.
[59] Callow KA, Parry HF, Sergeant M, Tyrrell DA. The time course of the immune response to experimental coronavirus infection of man. Epidemiol Infect 1990;105(2):435–46. http://dx.doi.org/10.1017/s0950268800048019.
[60] Mo H, Zeng G, Ren X, Li H, Ke C, Tan Y, et al. Longitudinal profile of antibodies against SARS-coronavirus in SARS patients and their clinical significance. Respirology 2006;11(1):49–53. http://dx.doi.org/10.1111/j.1440-1843.2006.00783.x.
[61] Sistema Estadual de Anáse de Dados - SEADE. SP contra o novo coronavírus boletim completo. 2021, https://www.seade.gov.br/coronavirus/. [Accessed 06 April 2021].
[62] Golnaraghi DF, Kuo DBC. Automatic control systems. 10th ed.. New York: McGraw-Hill Education; 2017.
[63] Chen X, Huang H, Ju J, Sun R, Zhang J. Impact of vaccination on the COVID-19 pandemic in U.S. states. Sci Rep 2022;12(1):1554. http://dx.doi.org/10.1038/s41598-022-05498-z.
[64] Aruffo E, Yuan P, Tan Y, Gatov E, Moyles I, Bélair J, et al. Mathematical modelling of vaccination rollout and NPIs lifting on COVID-19 transmission with VOC: a case study in Toronto, Canada. BMC Public Health 2022;22(1):1349. http://dx.doi.org/10.1186/s12889-022-13597-9.
[65] Diekmann O, Heesterbeek JAP, Roberts MG. The construction of next-generation matrices for compartmental epidemic models. J R Soc Interface 2009;7(47):873–85. http://dx.doi.org/10.1098/rsif.2009.0386.
[66] Abioye AI, Peter OJ, Oguntolu FA, Adebisi AF, Aminu TF. Global stability of SEIR-SEI model of malaria transmission. Adv Math Sci J 2020;9(8):5305–17. http://dx.doi.org/10.37418/amsj.9.8.2.
[67] Sistema Estadual de Análise de Dados - SEADE. Portal de estatísticas do Estado de São Paulo. 2020, http://www.imp.seade.gov.br. [Accessed 19 June 2020].
[68] Sistema Estadual de Análise de Dados - SEADE. SP contra o novo coronavírus boletim completo - Estado SP. 2021, https://www.seade.gov.br/coronavirus/. [Accessed 20 April 2021].
[69] Giordano G, Blanchini F, Bruno R, Colaneri P, Di Filippo A, Di Matteo A, Colaneri M. Modelling the COVID-19 epidemic and implementation of population-wide interventions in Italy. Nat Med 2020;26(6):855–60. http://dx.doi.org/10.1038/s41591-020-0883-7.
[70] Prem K, Liu Y, Russell T, Kucharski A, Eggo R, Davies N, et al. The effect of control strategies to reduce social mixing on outcomes of the COVID-19 epidemic in Wuhan, China: a modeling study. Lancet Public Health 2020;5(5):e261–70. http://dx.doi.org/10.1016/S2468-2667(2030073-6).
[71] Ferguson NM, Laydon D, Nedjati-Gilani G, Imai N, Ainslie K, Baguelin M, et al. Report 9: Impact of non-pharmaceutical interventions (MPIs) to reduce COVID-19 mortality and healthcare demand. In: Imperial college COVID-19. 2020, p. 1–20. http://dx.doi.org/10.25561/77482.
[72] Sistema Estadual de Análise de Dados - SEADE. SP contra o novo coronavírus adesão ao isolamento social em SP. 2021, https://www.saopaulo.sp.gov.br/coronavirus/isolamento/. [Accessed 30 April 2021].
[73] Conn AR, Gould NIM, Toint PL. Trust region methods. Society for Industrial and Applied Mathematics; 2000, http://dx.doi.org/10.1137/1.9780898719857.
[74] Moré JJ, Sorensen DC. Computing a trust region step. SIAM J Sci Stat Comput 1983;4(3):553–72. http://dx.doi.org/10.1137/0904038.
[75] Lima TM, Palamim CVC, Melani VF, Mendes MF, Pereira LR, Marson FAL. COVID-19 underreporting in Brazil among patients with severe acute respiratory syndrome during the pandemic: An ecological study. Diagnostics 2022;12(6):1505. http://dx.doi.org/10.3390/diagnostics12061505.
[76] Sansone NMS, Boschiero MN, Marson FAL. Epidemiologic profile of severe acute respiratory infection in Brazil during the COVID-19 pandemic: An epidemiological study. Front Microbiol 2022;13. http://dx.doi.org/10.3389/fmicb.2022.911036.
[77] Singh A, Chattopadhyay A. COVID-19 recovery rate and its association with development. Indian J Med Sci 2021;73:8–14. http://dx.doi.org/10.25259/IJMS_229_2020.
[78] Statista. Number of coronavirus COVID-19 cases, recoveries, and deaths worldwide. 2022, https://www.statista.com. [Accessed 15 Auguest 2022].
[79] Instituto Brasileiro de Geografia e Estatística - IBGE. Estado de São Paulo. 2022, https://www.ibge.gov.br/. [Accessed 15 Auguest 2022].
[80] Sistema Estadual de Análise de Dados. Portal de Estatísticas do Estado de São Paulo. 2021, http://www.imp.seade.gov.br/frontend/#/tabelas. [Accessed 12 Auguest 2021].
[81] Kifle ZS, Obsu LL. Mathematical modeling for COVID-19 transmission dynamics: A case study in Ethiopia. Results Phys 2022;34:105191. http://dx.doi.org/10.1016/j.rinp.2022.105191.
[82] Acheampong E, Okyere E, Iddi S, Bonney JH, Asamoah JKK, Wattis JA, et al. Mathematical modelling of earlier stages of COVID-19 transmission dynamics in Ghana. Results Phys 2022;34:105193. http://dx.doi.org/10.1016/j.rinp.2022.105193.
[83] Tillett R, Sevinsky J, Hartley P, Kerwin H, Crawford N, Gorzalski A, et al. Genomic evidence for a case of reinfection with SARS-CoV-2: a case study. Lancelet Infect Dis 2021;21(1):52–8. http://dx.doi.org/10.1016/S1473-3099(2030764-7).
[84] Johnston C, Hughes H, Lingard S, Hailey S, Healy B. Immunity and infectivity in COVID-19. BMJ 2022;e061402. http://dx.doi.org/10.1136/bmj-2020-061402.
[85] Sciscent BY, Eisele CD, Ho L, King SD, Jain R, Golamari RR. COVID-19 reinfection: the role of natural immunity, vaccines, and variants. J Commun Hosp Intern Med Perspect 2021;11(6):733–9. http://dx.doi.org/10.1080/20009666.2021.1974665.
[86] National Health Service - NHS - UK. COVID-19 symptoms and what to do. 2021, https://www.nhs.uk/conditions/coronavirus-covid-19/self-isolation-and-treatment/when-to-self-isolate-and-what-to-do/. [Accessed 20 March 2021].
[87] Abebe HT, Ashebir MM, Ebrahim MM, Zelelow YB, Bezabih AM, Tefere GR, et al. Epidemiological and clinical characteristics of COVID-19 patients in northern Ethiopia: A retrospective cohort study. Infect Drug Resist 2022;15:3579–88. http://dx.doi.org/10.2147/IDR.S345936.
[88] Grassly NC, Fraser C. Seasonal infectious disease epidemiology. Proc R Soc B Biol Sci 2006;273(1600):2541–50. http://dx.doi.org/10.1098/rspb.2006.3604.
[89] Cidade de São Paulo - Saúde. Boletins Secretaria Municipal da Saúde. 2023, https://www.prefeitura.sp.gov.br/cidade/secretarias/saude/vigilancia_e_saude/index.php?p=295572/. [Accessed 08 Februrary 2023].